THE EFFECT OF STACKING SEQUENCE ON THE LOW-VELOCITY IMPACT RESPONSE OF COMPOSITE LAMINATES

N. Hongkarnjanakul[1*], C. Bouvet[1], S. Rivallant[1]

[1]*Université de Toulouse; ISAE, INSA, UPS, EMAC; ICA (Institut Clément Ader) – ISAE, 10 avenue Edouard Belin, 31055 Toulouse Cedex 4, France*
**n.hongkarnjanakul@isae.fr*

Keywords: composite, impact damage, stacking sequence, damage tolerance

Abstract
Stacking sequence is an important effect in optimizing composite structures subjected to the low-velocity impact. This paper presents 7 out of 12 possible configurations made of 8-double-ply, mirror-symmetric, quasi-isotropic, T700GC/M21 laminated plates, oriented at 0°, 90°, 45° and -45°. Thanks to discrete modelling with interface finite elements based on fracture mechanics, a finite element model simulates impact damage. The numerical simulations can well predict the impact damage observed in experiments. Comparison of stacking sequence effect in term of areas and shapes of delamination, and fibre failures are discussed.

1. Introduction
Low-velocity impact on composite structures can reduce their strength up to 50% [1]. In order to improve impact resistance, changing stacking sequence can be one of the most effective factors [2-4]. After being impacted, the structures should be able to withstand other load cases during their service life until the impact damage has been detected. Compression After Impact (CAI) is often considered because it is more destructive than other load cases. This leads to overall concept of impact damage tolerance optimization. Thus, a proposed stacking sequence must have good properties to resist not only out-of-plane load from impact, but also in-plane load after impact. Many pieces of research on the effect of stacking sequence on low-velocity impact have been elaborated both in experimental and numerical studies. Fouss et al. [2], investigating delamination of stacking sequences with different parametric studies of quasi-isotropic layups, found that damage areas would not relatively high if the interface angle is in range between 30° to 75°, as well as suggesting to avoid ply-grouping. However, this FE model was based on linear quasi-static analysis instead of dynamic impact analysis. Hitchen and Kemp [3] recommended placing ±45° plies on the laminated outer surface in order to reduce delamination areas, which directly affect CAI strength. Lopes et al. [4-5] studied a traditional layup, combining 0°, 90°, 45° and -45° plies. To improve the impact resistance, two alternative layups with non-traditional orientations such as 5°, 15°, 70°, were tested. Lopez et al reported that the alternative layups had unobvious improvement on impact resistance; nevertheless, the FE model could present a good correlation between impact damage and dissipated energy - even though it consumed time and processing power, approximately 5-6 days with 32 CPUs.

This research is supplementary work from Bouvet et al. [6-7], who have been developing impact FE models aiming to impact damage tolerance and permanent indentation. In order to ensure the robustness of the reference models in [6-7] and to carry on optimizing composite structures, the effect of stacking sequence is taken into account. The reference stacking sequence is an 8-double-ply, mirror-symmetric, quasi-isotropic laminated plate of T700GC/M21 (carbon/epoxy): $[0°_2, 45°_2, 90°_2, -45°_2]_{sym}$, which contains equal number of ply in each orientation. It should be noted that, in the reference stacking sequence, double-ply in same orientation are bonded together to facilitate impact damages observation and to facilitate FE model simulation, which is currently not applied for industrial purpose. In this research, the effect of changing stacking sequences based on the reference layup will be studied.

Both experimental and numerical FE model results will be presented in this paper. However, the permanent indentation and the CAI will be not included. The main objective of switching stacking sequences is to numerically optimize the structures due to impact resistance. The impact damage will be observed and modelled to improve the material law of fibre failure, matrix cracking and delamination. Following the study, an appropriate position of each ply orientation should be guided for the purpose of having less impact damage and gaining better CAI resistance. Moreover, the simulation could also give a better understanding of impact damage phenomena.

2. Experimental study and specimen configurations

Impact tests were performed in drop tower system with an impactor of 16 mm diameter and 2 kg, according to Airbus Industries Test Method (AITM 1-0010) [13]. In each impact test, approximate impact energy is set to the height of drop weight in term of potential energy. Before impacting onto the specimen, the initial velocity is measured by an optical laser. Also, a force sensor is placed inside the impactor in order to measure contact force during the impact. All data are recorded in an oscilloscope Yokokawa DL708. The impact energy can then be confirmed by integration of force and vertical displacement (plate deflection), which also allows for evaluating dissipated energy. The dimension of rectangular specimen is $100 \times 150 \times 4.16$ mm^3 simply supported on a 75×125 mm^2 window, as shown in Figure 1.

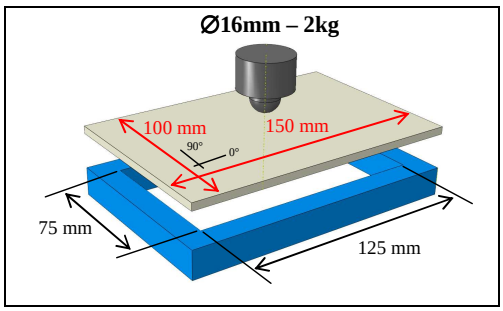

Figure 1 Impact test setup with the boundary condition

According to the reference case, 8-double-ply layup (0.26 mm nominal ply thickness) of UD carbon-epoxy T700GC/M21 were manufactured on 0°, 90°, 45° and -45°. Thanks to mirror-symmetric consideration, changing ply orientation allows having 24 possible configurations. The results will be duplicated because they are symmetry along longitudinal axis. Therefore, they were then reduced to 12 study cases. However, to reduce the manufacturing process, only 7 configurations were experimentally tested, as summarized in Table 1. Two specimen configurations having 90°-rotated are named with the same beginning letter, listed in Table 1. The quasi-isotropic reference layup A1 contains plies stacked at a constant interface angle of 45°. However, when ply orientation is changed, interface angle of 90° becomes unavoidable

in the layups B1, B2, C1, C2, E1 and E2. Therefore, the effects of interface angle 45° and 90°, which affect total impact damage, will also be studied. Delamination areas are observed by ultrasonic C-scan technique, and a major fibre failure can be indicated at dramatic load drop in force-time curve. The lamina properties of the material from [11-12] are summarized in Table 2

Layup Name	Stacking sequences	Experiment	Remarks
A1	$[0°_2, 45°_2, 90°_2, -45°_2]_{sym}$	✓	*Reference case*
A2	$[90°_2, -45°_2, 0°_2, 45°_2]_{sym}$		*90° rotation of A1*
B1	$[0°_2, 45°_2, -45°_2, 90°_2]_{sym}$		
B2	$[90°_2, -45°_2, 45°_2, 0°_2]_{sym}$		*90° rotation of B1*
C1	$[0°_2, 90°_2, 45°_2, -45°_2]_{sym}$	✓	
C2	$[90°_2, 0°_2, -45°_2, 45°_2]_{sym}$	✓	*90° rotation of C1*
D1	$[45°_2, 0°_2, -45°_2, 90°_2]_{sym}$	✓	
D2	$[-45°_2, 90°_2, 45°_2, 0°_2]_{sym}$	✓	*90° rotation of D1*
E1	$[45°_2, -45°_2, 90°_2, 0°_2]_{sym}$	✓	
E2	$[-45°_2, 45°_2, 0°_2, 90°_2]_{sym}$	✓	*90° rotation of E1*
F1	$[45°_2, 0°_2, 90°_2, -45°_2]_{sym}$		
F2	$[-45°_2, 90°_2, 0°_2, 45°_2]_{sym}$		*90° rotation of F1*

Table 1 Total possible stacking sequences with 7 experimental tested cases

E_l^{trac} (GPa)	E_l^{comp} (GPa)	E_t (GPa)	G_{lt} (GPa)	υ_{lt}	σ_t^{rupt} (MPa)	τ_{lt}^{rupt} (MPa)
130	100	7.7	4.8	0.33	60	110

Table 2 Mechanical properties of T700GC/M21 unidirectional ply

where, for a ply, $E_l^{trac}, E_l^{comp}, E_t, G_{lt}, \upsilon_{lt}$ are the Young's modulus in tension in fibre direction, the Young's modulus in compression in fibre direction, the transversal Young's modulus, the shear modulus, and the Poisson's ratio. $\sigma_t^{rupt}, \tau_{lt}^{rupt}$ are the transversal strength, and the in-plane shear strength, respectively.

3. Numerical Modelling

In previous study, Bouvet et al. [6-7] presented a discrete 3-dimension model of impact with particular mesh construction, oriented in 0°, 90°, 45° and -45°, as illustrated in Figure 2b. Positions of nodes are uniformly stacked in row and column for all oriented plies. However, the shapes of mesh are different: 0° and 90° plies are meshed in square shape, while 45° and -45° plies are meshed in parallelogram shape in order to follow the fibre direction. The model is simulated in explicit/dynamic response in Abaqus v6.9 with user subroutine Vumat. According to experimental observation, impact damages can be separately modelled in (i) fibre failure, (ii) matrix cracking in intra-ply and (iii) delamination between plies, as shown in Figure 2a.

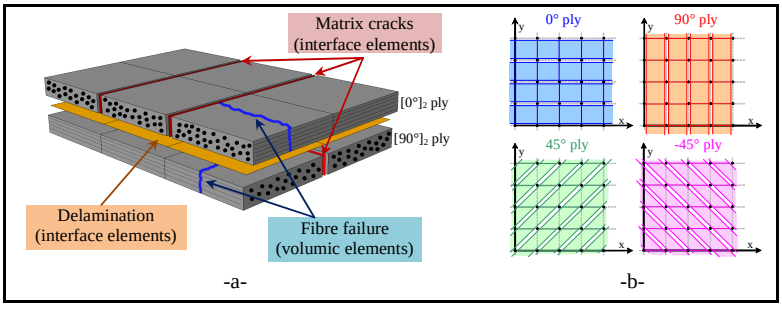

Figure 2 Model of (a) impact damages and their element types; and (b) mesh shapes in each oriented ply [6]

3.1 Modelling of fibre failure

A double-ply, modelled in volumic element, is able to represent the fibre failure, as illustrated in Figure 2a. The failure criterion of fracture mechanics in mode I is applied at each Gauss point inside the volumic element. As presented in Figure 3a, beginning with elastic behaviour to the damage initiation (i) driven by the failure strain (ε_0). The strain at each Gauss points is extrapolated to their nodes. As soon as the strain at one of the eight nodes reaches the failure strain (Eq.1), all of the strains at the eight integration points will turn to the damage propagation state (ii) even if the rest have not yet reached the failure strain. In this state, thanks to the critical energy release rate (G_{Ic}^{fibre}), the fracture mechanics allow dissipating energy by combining the energy together at all Gauss points until reaching total propagation damage. The equation of this relation is presented in Eq.2.

$$\max\left(\varepsilon_{node}^{i}\right) = \varepsilon_0 \tag{1}$$

$$\sum_{i=1}^{8} \frac{V}{8} \cdot \int_0^{\varepsilon_1^i} \sigma_l^i \cdot d\varepsilon_l^i = S \cdot G_{Ic}^{fibre} \tag{2}$$

where, at each Gauss point, $\sigma_l^i, \varepsilon_l^i, \varepsilon_1^i$ are the longitudinal stress, the longitudinal strain, the strain at total propagation, respectively. V, S are the volume and the cross section of an element normal to the fibre direction, G_{Ic}^{fibre} is the critical energy release rate of fibre.

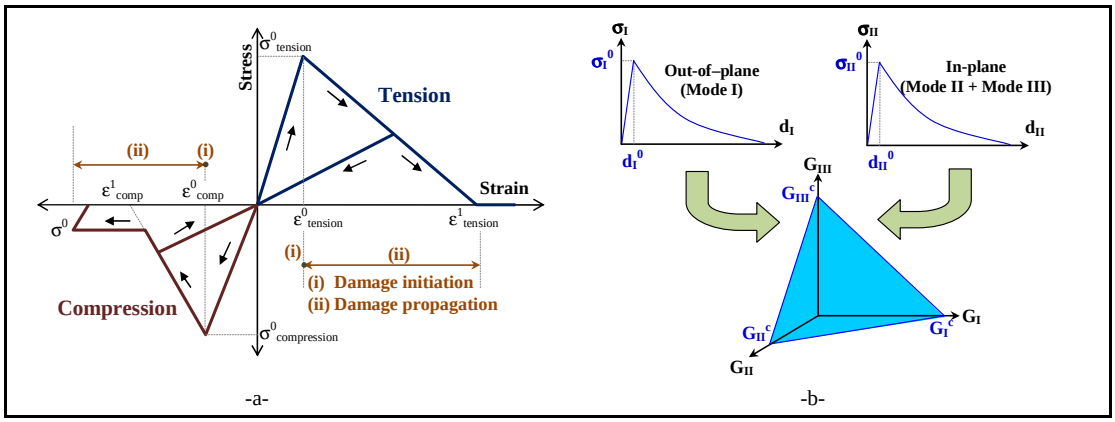

Figure 3 Behaviour laws of (a) fibre failure in longitudinal direction;
(b) delamination of linear coupling fracture in 3 modes [7]

This fibre failure law is used for both tension and compression. For the compression, a crushing plateau stress (σ^0) of -200 MPa is added, as shown in Figure 3a. According to the complexity of damage propagation in compression fibre failure [9] and to avoid an excess energy dissipation, an artificial critical energy release rate in compression (see Table 3) is introduced which is mostly dissipated in the damage initiation.

3.2 Modelling of matrix cracking

A particular modelling of matrix cracking is introduced using interface elements between two volumic elements, which are normal to the transverse direction and parallel to the fibre direction, as illustrated in Figure 2a. Quadratic classic criterion of matrix cracking (Eq.3) is then applied in the volumic elements. As soon as this criterion is reached either one or both neighbouring volumic elements of the interface element, the stresses in the interface elements are turned to zero, meaning that the matrix is broken.

$$\left(\frac{\langle\sigma_t\rangle^+}{\sigma_t^{rupt}}\right)^2 + \frac{(\tau_{lt})^2+(\tau_{tz})^2}{\left(\tau_{lt}^{rupt}\right)^2} \leq 1 \quad (3)$$

where material properties are mentioned in Table 2. In addition to the matrix cracking, these interface elements can also be used to model the permanent indentation (see more details in [6]).

3.3 Modelling of delamination

In general, the formation of delamination interacts with matrix cracking [1, 6-7]. For this present discrete modelling, even if there is no coupling parameter of delamination and matrix cracking, the discontinuity allows to have this interaction. Delamination is normally formed between different orientation plies. It is therefore simulated on interface elements, joining nodes of lower and upper volumic ply elements. Thanks to energy dissipation of fracture mechanics, the criterion of delamination is simulated as linear coupling in 3 modes: mode I is in the thickness direction normal to delamination plane, while mode II and mode III are in-plane direction [6], as shown in Figure 3b.

$$\frac{G_I}{G_{Ic}^{del}} + \frac{G_{II}}{G_{IIc}^{del}} + \frac{G_{III}}{G_{IIIc}^{del}} = 1 \quad (4)$$

where G_I, G_{II}, G_{III} are the energy release rate of delamination in mode I, II and III, respectively. $G_{Ic}^{del}, G_{IIc}^{del}, G_{IIIc}^{del}$ are the critical energy release rate of delamination in mode I, II and III, respectively. Material properties of T700GC/M21 from [8-11], which are used for the modelling, are summarized in Table 3.

Fibre failure				**Delamination**	
ε_l^{trac}	ε_l^{comp}	$G_{Ic}^{fibre,trac}$ (N/mm^2)	$G_{Ic}^{fibre,comp}$ (N/mm^2)	G_{Ic}^{del} (N/mm^2)	G_{IIc}^{del} (N/mm^2)
0.016	-0.0125	133	10	0.6	2.1

Table 3 Material properties of T700GC/M21 for numerical simulation

Then, damage variable of the delamination, representing the delamination areas in each interface layer, can be exported and overlaid, similar to the experimental C-scan, called "numerical C-scan".

4. Experimental validation of modelling

Tests were carried out at 25J of impact energy, since the impact damage at this energy level can be clearly seen both fibre failure and delamination. The results from numerical simulations are in good agreement with experiments for all different stacking sequences. The calculation time of this model is approximately 4-5 hours with 8 CPUs. Comparisons of experiments and numerical simulations are presented as the followings:

4.1 Fibre failure and impact response

During impact response, major fibre failure can be considered as a dramatic load drop in force-time curves, as presented in Figure 4. For example, case D1 and D2 can be obviously seen the dramatic load drop both in experiments and numerical simulations between 4-5 mm of displacement. From numerical observation, this phenomenon is induced by fibre failure in tension under impactor at the plies between the middle plane and non-impacted side, as shown in Figure 5c. Moreover, the fibre failure in compression, normally occurred only in small area under impactor, has less destructive effect than in tension, as showed in Figure 5c.

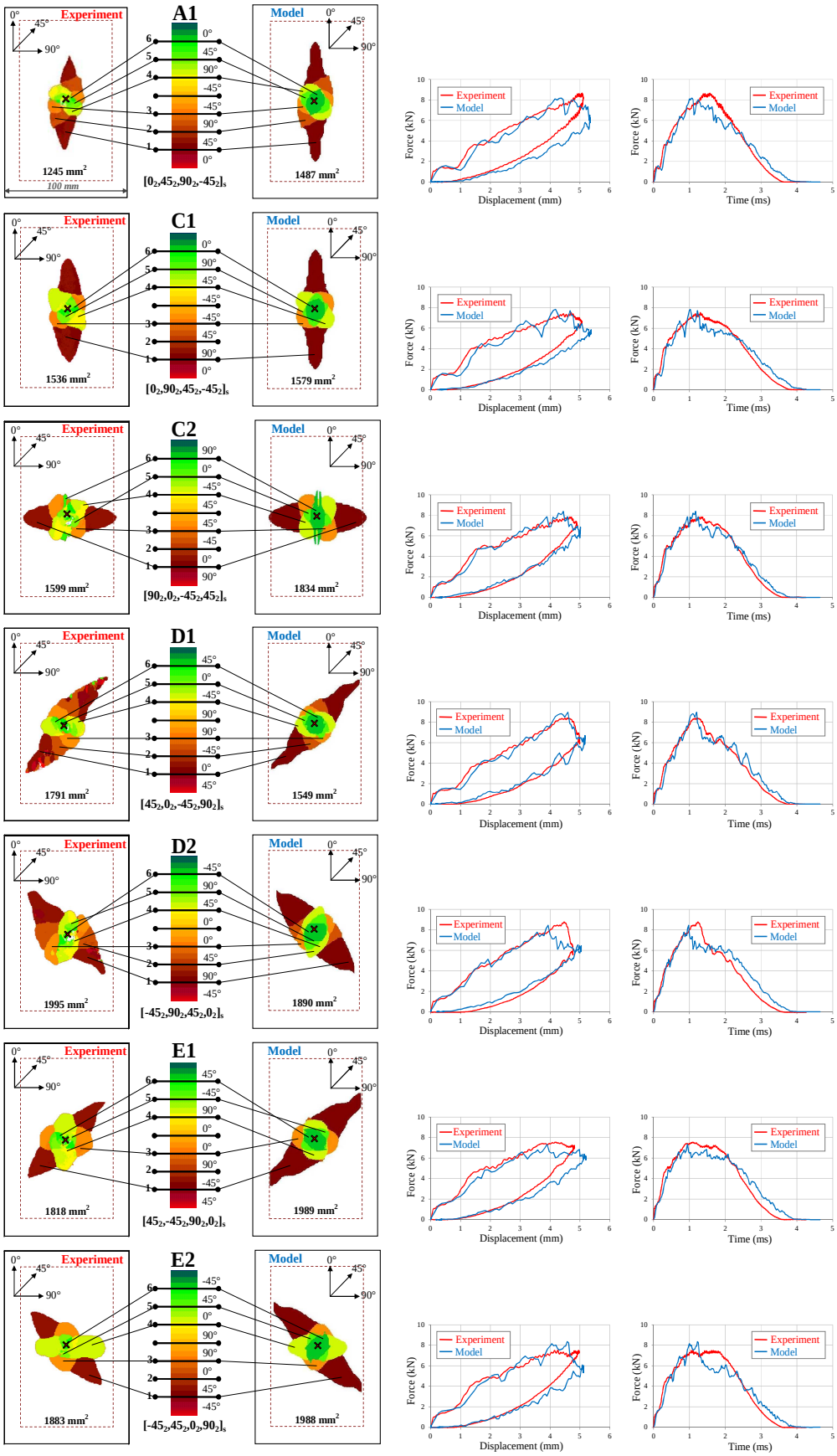

Figure 4 Comparison between experimental and numerical C-scan of delamination areas, force-displacement curves, and force-time curves of 25J impact tests.

Another interesting case is C2. It has 90° plies on the exterior, lying in small edge direction of the boundary condition. After being impacted, not only is permanent indentation observed. Also, a crack due to fibre failure on the upper surface (impacted side) appears due to the fibre failure in compression induced by bending effect, as shown in Figure 5(a-b). This confirms that the modelling of fibre failure in compression is necessary for impact damage. However, the compression fibre failure in this model may be overestimated for other stacking sequences, thus the behaviour law of fibre failure still needs to be improved.

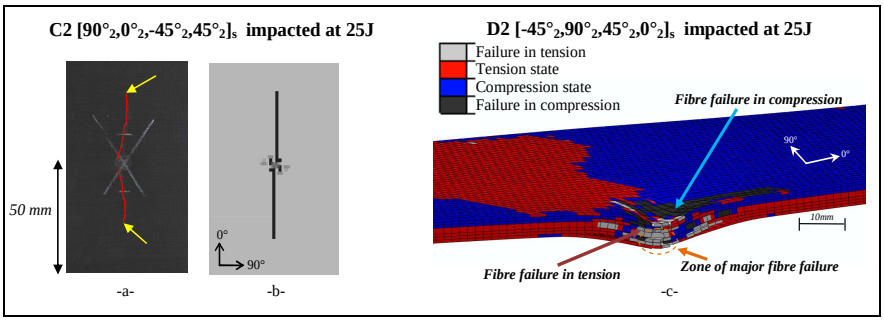

Figure 5: Compression fibre failure of impact 25J in case C2 [90°$_2$, 0°$_2$, -45°$_2$, 45°$_2$]$_s$: (a) crack from experiment; (b) damage variable fibre failure in the model; (c) fibre failure in tension and compression during impact at maximum deflection in case D2 [-45°$_2$, 90°$_2$, 45°$_2$, 0°$_2$]$_s$

4.2 Delamination

In experimental, delamination areas are obtained by ultrasonic C-scan technique. In general, delamination areas are dominant in the first interface at non-impacted side. Besides, delamination shape at each interface is always oriented in the fibre direction of lower ply, which is in accordance with the numerical simulations, as showed in Figure 4. For the two laminated configurations that have 90° rotation, i.e. C1-C2, D1-D2 and E1-E2, it can be remarked that the delamination shape seems as it turns 90° of another one. It means that the delamination will form in the same manner regardless of the boundary condition. However, the delamination area may still be different such as case D1-D2; and this assumption might be true for certain impact energy which is not too high. For the effect of interface angle, the cases that have both 45° interface and 90° interface, namely C1, C2, E1 and E2, are focused. It can be noticed that delamination is more dominant on 90° interface, clearly seen in case E1 and E2 (Figure 4) – also, the delamination of 45° interface is almost invisible. It means that when 45° interface and 90° interface are stacked together, the delamination is possibly occurred on 90° interface rather than 45° interface.

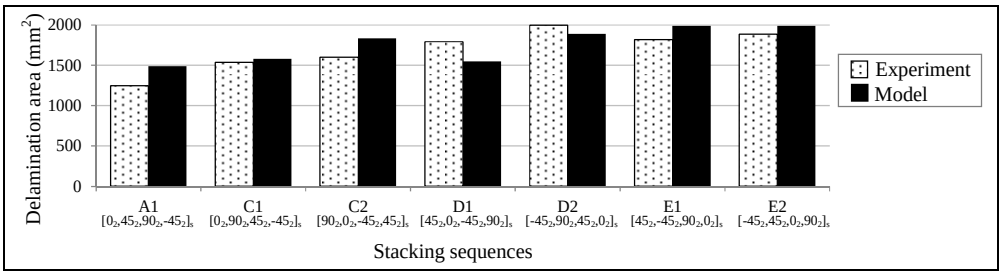

Figure 6 Comparison of delamination area in different stacking sequences

Figure 6 shows the comparison of delamination areas. Firstly, the numerical simulation is in good agreement with the experiments. Secondly, the different stacking sequences demonstrate the variation on delamination. For the case E1 and E2, placing ±45° on outer surface may improve the impact damage in term of fibre failures but not for delamination. According to these 7 studied configurations, case A1 with 0° on the exterior and a constant interface angle

of 45° seems to be the best stacking sequence for impact resistance because there is no major fiber failure, as well as having small delamination area. Further study in CAI is, however, needed in order to prove that fibre failures and delamination have essential influence on impact resistance.

5. Conclusion

With the same conditions, impact damages obviously depend on the stacking sequences. It can be represented mainly in delamination area and fibre failure. Numerical simulations show good agreement with the experimental results for all cases. It means that this model improvement is robust and could well simulate the impact damages even in different stacking sequence configurations. To complete this study, all 12 possible stacking sequences will be simulated and compared with each other. After the current results, CAI experiments and CAI simulations need to be performed in order to obtain the residual strength after impact. Finally, the robust model will be able to use to numerically optimize the stacking sequence in any configurations for industrial purpose to cut cost in manufacturing process.

References

[1] Richardson M. O. W., Wilsheart M. J., Review of low-velocity impact properties of composite materials. *Composites Part A*, **27A**, pp. 1123-1131 (1996).

[2] Fuoss E., Straznicky P. V., Poon C., Effects of stacking sequence on the impact resistance in composite laminates - Part 1: parametric study. *Composite Structures*, **41**, pp. 67-77 (1998).

[3] Hitchen, S. A., Kemp R. M. J., The effect of stacking sequence on impact damage in a carbon fibre/epoxy composite. *Composites*, **26**, pp. 207-214 (1995).

[4] Lopes C. S., Seresta O., Coquet Y., Gürdal Z., Camanho P. P., Thuis B., Low-velocity impact damage on dispersed stacking sequence laminates - Part I: Experiments. *Composites Science and Technology*, **69**, pp. 926-936 (2009).

[5] Lopes C. S., Camanho P. P., Gürdal Z., Maimí P., González E. V., Low-velocity impact damage on dispersed stacking sequence laminates - Part II: Numerical Simulations. *Composites Science and Technology*, **69**, pp. 937-947 (2009).

[6] Bouvet C., Castanié B., Bizeul M., Barrau J.-J., Low velocity impact modelling in laminate composite panels with discrete interface elements. *International Journal of Solids and Structures*, **46**, pp. 2809-2821 (2009).

[7] Bouvet C., *Impact damages on composite laminate*, in "Proceeding of *17èmes Journées Nationales sur les Composites*", Poitiers, France, (2011).

[8] Tomblin J., Sherraden J., Seneviratne W., Raju K. S., *A – Basis and B – Basis Design Allowables for Epoxy – Based Prepreg TORAY T700GC-12K-31E/#2510 Unidirectional Tape* in "Advanced General Aviation Transport Experiments", Wichita, Kansas, (2002).

[9] Pinho S.T., Robinson P., Iannucci L., Fracture toughness of the tensile and compressive fibre failure modes in laminated composites. *Composites Science and Technology*, **66**, pp. 2069-2079 (2006).

[10] Vandellos T., Hautier M., Huchette C., Carrère N., *A strategy to identify a cohesive zone model coupled with intralaminar damage* in "Proceeding of *14th European Conference on Composite Materials*", Budapest, Hungary, (2010).

[11] Prombut P., *Caractérisation de la propagation de délaminage des stratifies composites multidirectionnels*, PhD thesis, Toulouse (2007).

[12] Guillon D., Etude des mécanismes d'absorption d'énergie lors de l'écrasement progressif de structures composites à base de fibre de carbone, PhD thesis, Toulouse (2008).

[13] Airbus Industries Test Method : AITM 1-0010 : Determination of compression strength after impact